Chemical Geology 337–338 (2013) 56–66

Contents lists available at SciVerse ScienceDirect

Chemical Geology

journal homepage: www.elsevier.com/locate/chemgeo

Do carbonate precipitates affect dissolution kinetics? 2: Diopside

Gabrielle J. Stockmann [a,b,*], Domenik Wolff-Boenisch [c], Sigurdur R. Gislason [c], Eric H. Oelkers [b,c]

[a] Nordic Volcanological Center, Institute of Earth Sciences, University of Iceland, Sturlugata 7, 101 Reykjavík, Iceland
[b] GET-Université de Toulouse-CNRS-IRD-OMP, 14 Avenue Edouard Belin, 31400 Toulouse, France
[c] Institute of Earth Sciences, University of Iceland, Sturlugata 7, 101 Reykjavík, Iceland

ARTICLE INFO

Article history:
Received 16 April 2012
Received in revised form 15 November 2012
Accepted 23 November 2012
Available online 10 December 2012

Editor: U. Brand

Keywords:
Diopside
Calcite coating
Dissolution kinetics
Mixed-flow reactors
Carbonatization
CO_2 sequestration

ABSTRACT

Diopside dissolution rates were measured in mixed-flow reactors at neutral and basic pH at 25 °C and 70 °C. Experiments were performed in aqueous solutions 1) supersaturated with respect to calcite for up to 63 days, and 2) strongly undersaturated with respect to calcite and other secondary phases for up to 164 days. Inlet solutions were comprised of $NaHCO_3$, $CaCl_2$, NH_4Cl, NaOH, and/or HCl with ionic strengths ranging from 0.01 to 0.09 mol/kg. In the experiments performed at 25 °C, calcite nucleated and grew extensively on both the diopside surfaces, and as <1000 μm discrete crystals in experiments performed in CO_3-bearing inlet solutions but no precipitates were formed on or adjacent to the diopside in experiments performed in CO_3-free inlet solutions. Measured diopside dissolution rates in calcite precipitating experiments at 25 °C based on Si are both 1) time independent, and 2) equal to that of corresponding control experiments performed in $NaHCO_3$-free inlet solutions. These observations indicate that diopside dissolution rates are unaffected by the simultaneous precipitation of calcite. Calcite likely forms a porous coating on diopside, which allows ions from the dissolving diopside to be transported readily to the bulk fluid. It seems therefore likely that carbonate precipitation will not slow pyroxene dissolution during carbon storage efforts.

1. Introduction

A large number of recent studies have been aimed at providing the scientific basis for the in-situ carbonatization of CO_2 in an effort to attenuate the consequences of anthropogenic carbon emissions (e.g. Oelkers and Schott, 2005; McGrail et al., 2006; Wolff-Boenisch et al., 2006; Marini, 2007; Matter et al., 2007; Goldberg et al., 2008; Kelemen and Matter, 2008; Oelkers and Cole, 2008; Oelkers et al., 2008; Schaef and McGrail, 2009; Schaef et al., 2009, 2010, 2011; Wakahama et al., 2009; Flaathen et al., 2010; Gislason et al., 2010; Alfredsson et al., 2011; Aradóttir et al., 2011; Gysi and Stefansson, 2011; Matter et al., 2011; Rudge et al., 2011; Wolff-Boenisch et al., 2011; Aradóttir et al., 2012a, b; Gysi and Stefansson, 2012a,b,c). In-situ CO_2 carbonatization is promoted by the dissolution of silicate rocks that release divalent metal cations such as Ca^{2+}, Mg^{2+}, and Fe^{2+} to the fluid phase. These ions can react with dissolved CO_2 and precipitate as carbonate minerals. The rate-limiting step for CO_2 carbonatization is commonly thought to be the release of divalent cations (c.f., Oelkers et al., 2008). As such, any process that can potentially slow the dissolution rates of divalent metal bearing silicate minerals, such as secondary carbonate precipitation, could be detrimental to carbon storage efforts.

The dissolution rates of minerals and glasses are commonly believed to be proportional to their interfacial surface area (e.g. Pačes, 1983; Helgeson et al., 1984; Lasaga, 1984; Siegel and Pfannkuch, 1984; Schott and Oelkers, 1995; Oelkers, 2001; Schott et al., 2009). It seems likely therefore, that the precipitation of secondary phases, such as calcite during subsurface carbon storage efforts, could potentially decrease the dissolution rates of those phases on which they precipitate. Such precipitates could, therefore, be detrimental to mineral carbonatization efforts. This study is aimed at determining the extent to which diopside dissolution rates are affected by calcite precipitation on its surfaces. Towards this goal, diopside has been dissolved for up to 5 months in aqueous fluids that are either supersaturated or undersaturated with respect to calcite. The goal of this paper is to report the results of this experimental study and to use these results to assess the degree to which carbonate precipitation on silicate minerals might affect the efficiency of subsurface carbon storage efforts.

Diopside was chosen for this study of the potential effect of mineral coatings on mineral carbonation efforts for three major reasons. First, pyroxenes are an important source of the divalent cations required for mineral carbonation. Second, the presence of Ca in diopside could promote calcite precipitation during the experiments. Third, extensive studies of diopside dissolution are available in the literature for comparison (e.g. Schott et al., 1981; Eggleston et al., 1989; Knauss et al., 1993; Chen and Brantley, 1998; Golubev et al., 2005; Golubev and Pokrovsky, 2006; Dixit and Caroll, 2007; Daval et al., 2010). Knauss et al. (1993)

* Corresponding author at: Department of Earth Sciences, University of Gothenburg, Guldhetsgatan 5A, 413 20 Gothenburg, Sweden. Tel.: +46 762 622 111.
E-mail address: gjs3@hi.is (G.J. Stockmann).

0009-2541/$ – see front matter © 2012 Elsevier B.V. All rights reserved.
http://dx.doi.org/10.1016/j.chemgeo.2012.11.014

reported diopside dissolution rates as a function of pH at 25, 50, and 70 °C. Measured diopside dissolution rates decrease with increasing pH to at least pH ~ 7. At higher pH, rates are either pH independent or decrease weakly with increasing pH (Knauss et al., 1993; Golubev et al., 2005). Chen and Brantley (1998) reported diopside dissolution rates as a function of pH at 25 and 90 °C; these rates also decrease with increasing pH at pH < 7 but they are approximately one order of magnitude lower than corresponding rates reported in other studies. Chen and Brantley (1998) suggested that this difference was most likely due to their rates being normalized to the BET surface area of the post-experiment powders, whereas the majority of other studies normalized rates to the BET surface area of the initial solids. Knauss et al. (1993) reported that diopside dissolution rates are independent of aqueous CO_2 concentration. Daval et al. (2010) found that diopside dissolution rates varied significantly as a function of solution saturation state (ΔG_r) at acidic conditions and 90 °C.

A number of past studies have focused on the effect of mineral coatings on the dissolution rates of divalent metal bearing silicates, in part due to the significance of this process to the carbonatization of ultramafic and mafic rocks. These studies include efforts on basaltic glasses (Gysi and Stefansson, 2011; Stockmann et al., 2011; Gysi and Stefansson, 2012a,b,c), crystalline basalts (McGrail et al., 2006; Schaef et al., 2009, 2010, 2011), wollastonite (Daval et al., 2009a,b), olivine (Giammar et al., 2005; Béarat et al., 2006; Andreani et al., 2009; Daval et al., 2011), serpentine (Park and Fan, 2004), and anorthite (Hodson, 2003). These past studies provide ambiguous results; in some cases dissolution rates are unaffected by coatings, but in others significant effects are observed. The presence of carbonate precipitates on basaltic glass (Stockmann et al., 2011), olivine (Giammar et al., 2005), and wollastonite at acidic pH conditions (Daval et al., 2009a) was reported to have no effect on the dissolution rates of the primary minerals as these coatings formed discontinuous and porous layers. Similarly, Hodson (2003) observed that the presence of discontinuous iron-rich coatings had little effect on anorthite dissolution rates. In contrast, Daval et al. (2011) reported that olivine dissolution rates decreased by two orders of magnitude by the presence of an amorphous silicate layer. Daval et al. (2009a,b) reported that wollastonite dissolution rates were significantly decreased at neutral and basic conditions due to the presence of a surface coating consisting of amorphous silica and calcite. Park and Fan (2004) suggested that the presence of silica-rich layers inhibited serpentine dissolution rates. Both Béarat et al. (2006) and Andreani et al. (2009) reported that silica-rich layers on dissolving olivine surfaces slowed carbonate formation, and inhibited olivine dissolution. Based on the results of the experiments mentioned above and those of Cubillas et al. (2005), it seems likely that crystallographic properties might play an important role in this process, especially during the early stages of dissolution–precipitation. Cubillas et al. (2005) showed that $CaCO_3$ dissolution rates were strongly affected by otavite ($CdCO_3$) precipitation on its surface because there was a close structural match between the dissolving and precipitating phases. Putnis (2009) noted that the replacement of one mineral by another is closely related to the degree of epitaxy between the product phase and the parent surface, their molar volumes, and the relative solubilities of the phases involved. Similarly, Velbel (1993) emphasized that the molar volume ratio of product to reactant has to be > 1 to provide the volume needed to completely passivate the reactant surface. This study aims to provide further insight into this coupled process through a series of diopside dissolution experiments performed in the presence and absence of co-precipitating calcite.

2. Materials and methods

The standard state adopted in this study is that of unit activity of pure minerals and H_2O at any temperature and pressure. For aqueous species other than H_2O, the standard state is unit activity of the species in a hypothetical 1 mol/kg solution referenced to infinite dilution at any temperature and pressure. All thermodynamic calculations reported in this study were performed using the PHREEQC 2.17 computer code (Parkhurst and Appelo, 1999) together with its llnl.dat database.

The diopside crystals used in this study were obtained from the Transbaikal region of Russia and are identical to those studied by Golubev et al. (2005) and Golubev and Pokrovsky (2006). Golubev et al. (2005) determined the chemical composition of the diopside to be: $Ca_{0.99}Mg_{0.98}Fe_{0.02}Cr_{0.01}Si_2O_6$ with minor amounts of Al_2O_3 (0.15 wt.%), MnO (0.03 wt.%), Na_2O (0.4 wt.%), and TiO_2 (0.03 wt.%).

Prior to the experiments, the diopside crystals were reacted in concentrated HCl for several hours to remove impurities from the crystal surfaces. Following this acid cleaning, the diopside crystals were rinsed with MilliQ™ water and dried at 60 °C before being crushed with an agate mortar and pestle. After crushing, the material was sieved and the 45–125 μm size fraction was obtained. Fine particles were removed from this powder by ultrasonically cleaning in acetone. Several ultrasonic cleaning cycles were performed and the ultra-fine suspension was discarded at the end of each cycle. The cleaning cycles were repeated until the discarded fluid phase appeared clear. The resulting diopside powder was dried overnight at 60 °C. A representative Scanning Electron Microscope (SEM) image of this diopside powder is displayed in Fig. 1a, and this image shows the resulting diopside powder to be free of fine particles. All SEM images in this study were performed using a LEO Supra 25, JEOL 6360 LV or a HITACHI S3400N Scanning Electron Microscope after particles were coated with a fine gold layer. Further analysis of the solids in this study was performed using an Oxford Instruments INCA Energy Dispersive X-ray Spectrometer (EDS), and an INEL CPS 120 X-ray diffractometer (XRD).

The specific surface area of the cleaned dried diopside powder is 1013 ± 40 cm^2/g as determined by 3-point krypton adsorption using the BET method. Golubev et al. (2005) reported a BET specific surface area of 1250 ± 20 cm^2/g for their cleaned 50–100 μm size fraction of this diopside; Golubev and Pokrovsky (2006) reported a BET specific surface area of 1045 ± 50 cm^2/g for their cleaned 100–200 μm size fraction of this diopside. The average density of diopside, as reported by Klein (2002), is 3.27 g/cm^3. Taking account of this density and equations reported by Wolff-Boenisch et al. (2004a), the geometric surface area of the diopside used in this study, A_{geo}, is calculated to be 234 cm^2/g. Dividing the BET surface area by this geometric surface area yields a roughness factor of 4.3.

The mixed-flow reactor system used in this study is illustrated in Fig. 2. This reactor system is similar to that used in past dissolution rate measurement studies (e.g., Wolff-Boenisch et al., 2004a,b; Cubillas et al., 2005; Pokrovsky et al., 2005; Chaïrat et al., 2007; Gautelier et al., 2007). The physical and chemical conditions of the experiments performed in this study were identical to those of basaltic glass experiments described in Stockmann et al. (2011). All reactors, connectors, and tubing were cleaned in a 0.1 M HCl bath for ~24 h and rinsed with MilliQ™ water prior to each experiment. All outlet fluid sample bottles went through the same cleaning procedure prior to sampling to prevent contamination. Diopside dissolution experiments were initiated by placing between 5 and 10 g of cleaned diopside powder and a quantity of the selected inlet solution into the 300 mL polyethylene mixed-flow reactors. These reactors were sealed and placed into a temperature controlled water bath. Temperature was kept constant during the experiment at either 25 or 70 °C. Teflon® coated floating stir-bars from Nalgene™ were placed on the bottom of the reactors and rotated at ~300 rpm using a multi-position magnetic stirrer located underneath the water bath.

Inlet fluids were comprised of Millipore™ water and Merck/Sigma-Aldrich analytical grade $NaHCO_3$, $CaCl_2$, NH_4Cl, NaOH, and/or HCl with ionic strengths ranging from 0.01 to 0.09 mol/kg; the composition of all inlet fluids is listed in Table 1. Compositions of the inlet fluids were based on calculations made using PHREEQC to yield 1) the desired pH and ionic strength, 2) to achieve calcite saturation in the reactive fluids, and 3) to be similar to those that might be present during mineral carbonation efforts. The inlet fluids were stored in 8 or 12 L compressible

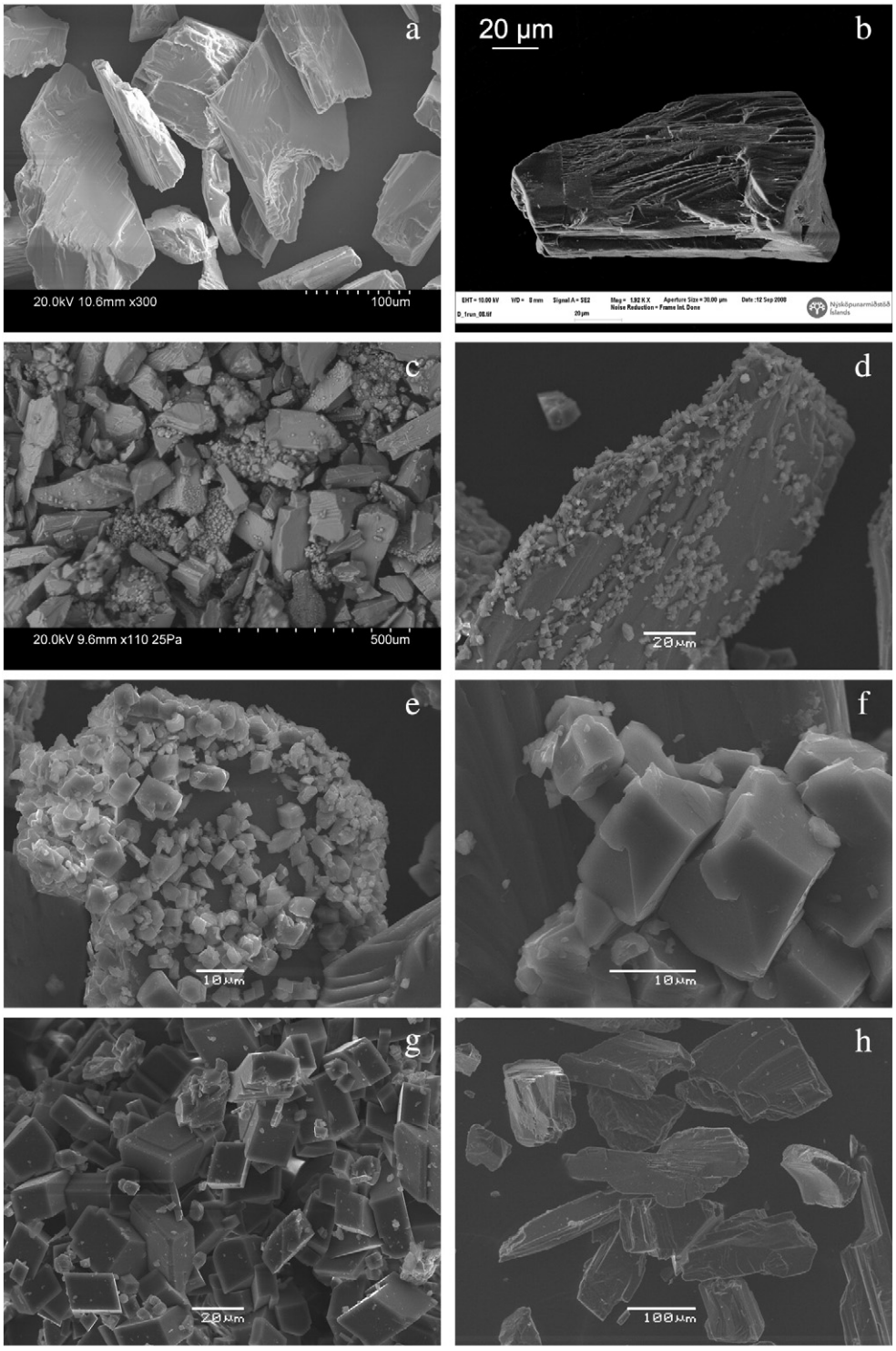

Fig. 1. Scanning electron images of diopside samples from this study. Image a) is of the cleaned diopside powder prior to experiments. Image b) is of a diopside grain after its dissolution during experimental series 1 for ~60 days at 70 °C. Images c–f) show secondary calcite precipitates growing on the surfaces of diopside following its dissolution during experimental series 4 at 25 °C and pH 7. Image f) is a close-up of image e) illustrating how the $CaCO_3$ crystals grow preferentially on topographical features ('surface ripples') on diopside surfaces. Image g) illustrates the morphology of $CaCO_3$ precipitates recovered from experimental series 4. Calcite clusters, like in g), ranged in size from 10 to 1000 µm. Image h) shows the surfaces of diopside following its dissolution for 164 days in control experimental series 5 at 25 °C.

plastic bags. Inlet fluids containing $CaCl_2$ were continuously purged with N_2 to prevent atmospheric CO_2 from dissolving into this fluid and to keep the pH stable. The inlet fluids were injected into the reactors at a constant rate using multi-cartridge Masterflex™ peristaltic pumps. In experiments at 70 °C, calcite saturation was sought by combining carbonate-rich inlet fluids with Ca^{2+} released from dissolving diopside. In the 25 °C experiments, two inlet fluids (one Ca-rich and one carbonate-rich) were injected simultaneously to create a reactive fluid supersaturated with respect to calcite in the reactor. The two inlet fluids had separate entrances into the reactor to avoid carbonate precipitation at or near the inlet.

Each experiment reported in this study was performed at a constant temperature, inlet fluid flow rate, and inlet fluid composition. All experiments were run until and beyond a steady-state outlet fluid composition

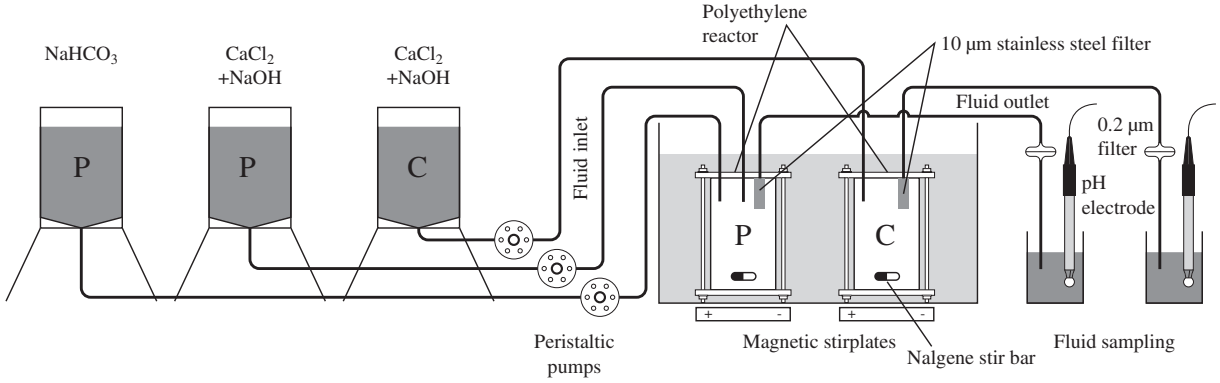

Fig. 2. Schematic illustration of the reactors used in the present study. Supersaturation of calcite in the precipitation experiments is obtained by mixing two inlet solutions comprised of $NaHCO_3$ and $CaCl_2$, respectively, inside the reactor. The control experiments ran with a $CaCl_2$ inlet solution designed to dissolve diopside without secondary precipitate formation. The 70 °C experiments were performed using an identical reactor system with only one inlet solution connected to the reactor comprised of $NaHCO_3$. In those experiments, diopside was the Ca-source in attempts to achieve calcite saturation inside the reactor.

was obtained. Steady-state is defined as the outlet fluid composition remaining constant, within analytical uncertainty, for at least 10 residence times. The residence time is defined as the reactor volume divided by the fluid flow rate. In selected experiments, the inlet fluid composition was changed after a steady-state concentration profile was attained. Two different types of experiments were performed: precipitation experiments and control experiments. These two types of experiments are distinguished by P and C respectively, in Table 1. Precipitation experiments were designed to measure diopside dissolution rates during carbonate precipitation. To achieve calcite saturation, carbonate ± calcium were provided to the system by the inlet fluids. Control experiments were designed to measure diopside dissolution rates at the same physical and chemical conditions as the corresponding precipitation experiment but in the absence of aqueous carbonate (see Table 1).

Outlet fluids were regularly sampled during all experiments. Three residence times or more separated each sampling. The outlet fluids were filtered through a 0.2 μm cellulose acetate membrane filter into 100 ml polyethylene sample bottles and acidified with concentrated supra-pure HNO_3 prior to analysis. The major element concentrations of inlet and outlet fluids were determined using a Spectro Ciros Vision Inductively Coupled Plasma Optical Emission Spectrometer (ICP-OES). Analytical uncertainties of ICP-OES analyses are estimated to be 3–5%.

At the end of the experiments, all diopside powders from the reactors were rinsed several times with 10 mM $NaHCO_3$ and then with MilliQ™ water, before being dried at 40 °C. After drying, the sample weight was recorded and the powders kept for SEM, EDS, and XRD analyses.

3. Experimental results

In total, 9 steady-state dissolution experiments and 2 short-term pH pulses at the end of selected dissolution experiments were performed as part of five experimental series. The chemical composition, pH, and ionic strength of the inlet fluids are listed in Table 1. Compositions of the outlet fluids at steady-state and calculated steady-state diopside dissolution rates for all 9 experiments are listed in Tables 2a and 2b together with the results of chemical speciation calculations. The saturation state of calcite and other selected minerals in the outlet fluids is provided in Table 3. The diopside dissolution rates based on the release of the *i*th element ($r_{+,i,j}$) listed in these tables were calculated from:

$$r_{+,i,j} = \frac{C_i \cdot fr}{\nu_i \cdot A_j \cdot m} \quad (1)$$

where C_i stands for the concentration of the *i*th element in the outlet fluid, *fr* refers to the fluid flow rate, ν_i represents the stoichiometric factor of the *i*th element, A_j designates the specific surface area of the diopside, and *m* denotes the mass of diopside used in the experiment. The index *j* refers to rates calculated either using the measured BET surface

Table 1
Composition of inlet fluids used in this study.

Experiment	Type of experiment[a]	$NaHCO_3$ (mol/kg)	NH_4Cl (mol/kg)	$CaCl_2$ (mol/kg)	NaOH (mol/kg)	HCl (mol/kg) [b]	Ionic strength (mol/kg)	pH (22 °C)	SI calcite
1a	P	0.035					0.035	8.45	
1b	P	0.035				n.m.	0.036	6.35	
2	P	0.035					0.035	8.54	
3	C	0.010					0.010	8.60	
4a [c]	P	0.035		0.010	1.2E−07		0.033	7.95 [d]	1.60[d]
4b [c]	P	0.035		0.020	1.6E−07		0.048	7.85 [d]	1.75[d]
5a	C			0.020	1.6E−07		0.060	7.92	
5b	C			0.030	1.7E−07		0.090	8.47	
5c [e]	C			0.030	1.7E−07		0.090	5.83	
5d	C	0.010					0.010	8.54	
5e	C		0.010			n.m.	0.010	3.81	

[a] P and C designates precipitation and control experiments, respectively.
[b] HCl was added until the desired pH was reached, but the exact concentration was not measured (n.m.).
[c] Two-inlet system, i.e. the concentration of the fluid entering the reactor is half of each inlet.
[d] Calculated at 25 °C using PHREEQC v. 2.17.
[e] The $CaCl_2$ powder used to make the inlet solution was Mg-free, whereas the $CaCl_2$ powder used in experiments 4a–b and 5a–b contained Mg as an impurity.

Table 2a
Physical conditions and steady-state results of the diopside dissolution experiments performed in this study.[a]

Exp.	T (°C)	m (g)	S_{BET} (m^2)	fr (g/min)	t_{exp} (days)	pH_{out} (22 °C)	pH_{out} in-situ T [b]	$[Si]_{out}$ (μmol/kg)	$[Ca]_{out}$ (μmol/kg)	$[Mg]_{out}$ (μmol/kg)	$[Fe]_{out}$ (μmol/kg)	$-\Delta G_r$ (kJ/mol) [b]
1a	70	10.00	1.01	0.56	53	8.74	8.46	15.36	5.61	5.70	0.013	36.4
1b [c]	70	10.00	1.01	0.55	6	7.30	7.19	23.38	11.84	13.28	b.d.	62.0
2	70	9.81	0.99	0.58	26	8.57	8.31	8.71	1.61	2.58	b.d.	49.0
3	70	4.67	0.47	1.13	13	8.58	8.29	3.68	0.87	1.23	b.d.	53.7
4a [d]	25	9.68	0.98	0.52	29	7.10	7.08	3.04	1942.38	9.11	0.030	67.9
4b [d]	25	9.68	0.98	0.50	34	6.91	6.89	1.45	5102.16	13.81	0.056	73.0
5a [d]	25	9.92	1.00	0.49	32	7.33	7.25	3.09	~20000	28.2	0.034	56.0
5b [d]	25	9.92	1.00	0.45	114	7.94	7.84	2.32	~30000	38.32	0.018	42.9
5c	25	9.92	1.00	0.47	18	6.37	6.34	2.00	~30000	1.54	0.008	85.4
5d	25	5.05	0.51	0.64	9	8.57	8.53	0.93	n.m.	1.07	b.d.	59.6
5e [c]	25	5.05	0.51	0.64	5	4.33	4.33	5.25	n.m.	2.67	0.076	142.3

n.m. = not measured.
b.d. = below detection limit.
[a] The data reported are the temperature (T), the initial mass of diopside (m), the initial BET surface area of the diopside (S_{BET}), the flow rate (fr), the total duration of the experiment (t_{exp}), measured pH of outlet solution, calculated pH of the outlet solution at in-situ T, the concentration of elements in the outlet solution in μmol/kg, and the chemical affinity of diopside ($-\Delta G_r$).
[b] Computed with PHREEQC version 2.17.
[c] pH pulse added at the end of experiment (end point data provided).
[d] The high Ca and Mg concentrations arise from the $CaCl_2$ powder used for making the inlet solution, which contained some Mg as an impurity.

area, A_{BET} or the geometric surface area, A_{geo}. These experimental results will be discussed in detail below.

3.1. Diopside dissolution in calcium ± carbonate-bearing aqueous fluids at 25 °C (experimental series 4 and 5)

The temporal evolution of diopside dissolution rates based on Si release at pH 6–8 and 25 °C in precipitation and control experiments is illustrated in Fig. 3. In the precipitation experiments, two inlet fluids were connected to the mixed-flow reactor; one injecting an aqueous 0.035 mol/kg $NaHCO_3$ solution and the other aqueous solution containing $CaCl_2$ and sufficient NaOH to attain the target pH, whereas the control experiment was run by injecting a single $CaCl_2$-bearing, CO_3-free aqueous solution. The precipitation experimental series 4a–b ran for 63 days in total. For the first 29 days the inlet fluid contained 0.1 mol/kg $CaCl_2$, and for the subsequent 34 days the inlet fluid contained 0.2 mol/kg $CaCl_2$. The control experimental series 5a–c ran for 164 days. For the first 32 days the inlet fluid contained 0.2 mol/kg $CaCl_2$, and for the next 132 days the inlet fluid contained 0.3 mol/kg $CaCl_2$. Experiments 5b and c are identical other than the pH in the latter was 1.5 units lower. Comparison of Fig. 3a and b shows that there is no significant difference in diopside dissolution rates observed between the control and the precipitation experiments, and the effect of changing $CaCl_2$ concentration in the inlet fluids had at most a small effect on measured rates. The steady-state diopside dissolution rate found in these experiments was $\log r_{+,Si,BET} = -15.1 \pm 0.15$ (mol/cm^2/s) and -15.2 ± 0.15 (mol/cm^2/s) for the control (5b–c) and precipitation (4b) experiments, respectively (see Table 2b). Calcite precipitation occurred during the precipitation experiments as seen in Fig. 1c–g. In general, calcite grew as discrete crystals on almost all diopside surfaces and some surfaces were completely overgrown with calcite (see Fig. 1c–e). Calcite was the only calcium carbonate phase present according to XRD analysis. This conclusion is confirmed by SEM photos showing that the precipitated phase consists of rhombohedral crystals consistent with calcite morphology (see Fig. 1e–g). SEM–EDS analysis showed that some of the calcite contains minor amounts of Mg (<0.5 wt.%). Mass balance calculations suggest that ~5 g of calcite was precipitated inside the reactor during the precipitation experiments. Precipitation occurred inside the reactor as well as in the outlet fluid tubing, which eventually clogged ending the experiment.

To evaluate the long-term dissolution behavior of diopside grains in fluids of different compositions, approximately half of the powder recovered from experiments 5a–c was subsequently returned to the mixed-flow reactor and reacted with a 0.01 mol/kg $NaHCO_3$ inlet fluid of pH 8.4 and 25 °C. After 9 days the inlet fluid was changed to a fluid having a pH of 3.81. The results of these experiments (5d and e) are illustrated in Fig. 4. Steady-state diopside dissolution rate in Exp. 5d, based on Si release is ~$10^{-15.0}$ mol/cm^2/s, whereas corresponding steady-state rate based on Mg release, is ~$10^{-14.6}$ mol/cm^2/s, consistent with a preferential release of Mg over Si at these conditions. The addition of the acid leads to an increase in instantaneous diopside dissolution rates to ~$10^{-14.3}$ mol/cm^2/s in Exp. 5e based on either Si, Mg and/or Fe release (see Table 2b), consistent with stoichiometric dissolution of diopside.

The variation of 25 °C diopside steady-state dissolution rates based on Si release with reactive fluid ionic strength, calcium concentration, and

Table 2b
Logarithms of measured steady-state diopside dissolution rates (r_+) in mol/cm^2/s based on the release rates of elected elements.

Exp.	T (°C)	pH_{out} at in-situ T	Log $r_{+,Si,BET}$	Log $r_{+,Si,geo}$	Log $r_{+,Ca,BET}$	Log $r_{+,Ca,geo}$	Log $r_{+,Mg,BET}$	Log $r_{+,Mg,geo}$	Log $r_{+,Fe,BET}$	Log $r_{+,Fe,geo}$
1a	70	8.46	−14.2	−13.5	−14.3	−13.6	−14.3	−13.6	−15.5	−14.8
1b [a]	70	7.19	−14.0	−13.3	−14.0	−13.3	−13.9	−13.3		
2	70	8.31	−14.4	−13.7	−14.8	−14.1	−14.6	−13.9		
3	70	8.29	−14.1	−13.5	−14.5	−13.8	−14.3	−13.6		
4a [b]	25	7.08	−14.9	−14.2					−15.1	−14.5
4b	25	6.89	−15.2	−14.6					−14.9	−14.2
5a [b]	25	7.25	−14.9	−14.2					−15.1	−14.5
5b	25	7.84	−15.1	−14.4					−15.4	−14.8
5c	25	6.34	−15.1	−14.5			−14.9	−14.3	−15.8	−15.1
5d	25	8.53	−15.0	−14.4			−14.6	−14.0		
5e [a]	25	4.33	−14.3	−13.6			−14.2	−13.6	−14.4	−13.7

[a] pH pulse added at the end of experiment (end point data provided).
[b] The steady-state dissolution rates listed here were calculated from the final measured reactive fluids compositions of these experiments.

Table 3
Saturation indices (SI) of selected minerals in the steady-state fluids in all experiments.[a,b,c]

Exp.	Calcite	Aragonite	Dolomite	Magnesite	Goethite	Hematite	$Fe(OH)_3$	SiO_2(a)	Chrysotile	Talc	Ca-saponite	Diaspore	Other minerals supersaturated according to modeling [a]
1a	−0.36	−0.51	0.89	−0.14	5.78	12.75	1.19	−2.57	−2.45	−3.66	−2.89	−1.06	Anatase, andradite, cronstedtite, ferrite, magnetite, nontronite, rutile, MnO_2
1b	−1.21	−1.36	−1.04	−1.22				−2.17	−9.05	−9.43	−8.72	0.28	Anatase, rutile
2	−1.02	−1.16	−0.23	−0.60				−2.77	−4.71	−6.30	−5.62	−1.12	Anatase, rutile
3	−1.43	−1.58	−1.24	−1.19				−3.15	−5.80	−8.15	−7.33	−1.12	Anatase, rutile
4a	0.25	0.11	−0.60	−2.48	3.29	7.56	−1.82	−2.64	−15.12	−15.83	−14.57	1.34	Anatase, magnetite, nontronite, dawsonite, boehmite, gibbsite, rutile
4b	0.43	0.29	−0.50	−2.56	2.94	6.86	−2.17	−3.10	−16.86	−18.51	−17.00	1.61	Anatase, magnetite, nontronite, dawsonite, boehmite, gibbsite, rutile
5a					3.55	8.09	−1.56	−2.78	−13.13	−14.13	−12.61	1.32	Gibbsite, anatase, boehmite, magnetite, nontronite, rutile
5b					3.49	7.97	−1.62	−2.91	−9.62	−10.87	−9.23	0.90	Gibbsite, anatase, boehmite, magnetite, nontronite, rutile
5c					0.98	2.94	−4.13	−2.96	−22.78	−24.14	−22.65	1.91	Gibbsite, anatase, boehmite, rutile
5d								−3.32	−10.67	−12.76			none
5e					−9.35	−17.71	−14.46	−2.53	−32.81	−33.31	−34.29	−1.53	none

[a] Computed with PHREEQC version 2.17.
[b] Saturation index is defined as: SI = log (IAP/K_{sp}), where IAP is the ion activity product and K_{sp} refers to the solubility product of the solid phase.
[c] Uncertainty is estimated to ±0.10 log unit.

diopside saturation state is illustrated in Fig 5. The distribution of data points in this figure suggests that there is no significant effect of these parameters on the steady-state diopside dissolution rates generated in this study at 25 °C. Within experimental uncertainty, all measured rates at pH 6–8 are equal to ~$10^{-15.1}$ mol/cm^2/s, as was also shown in Fig. 3b.

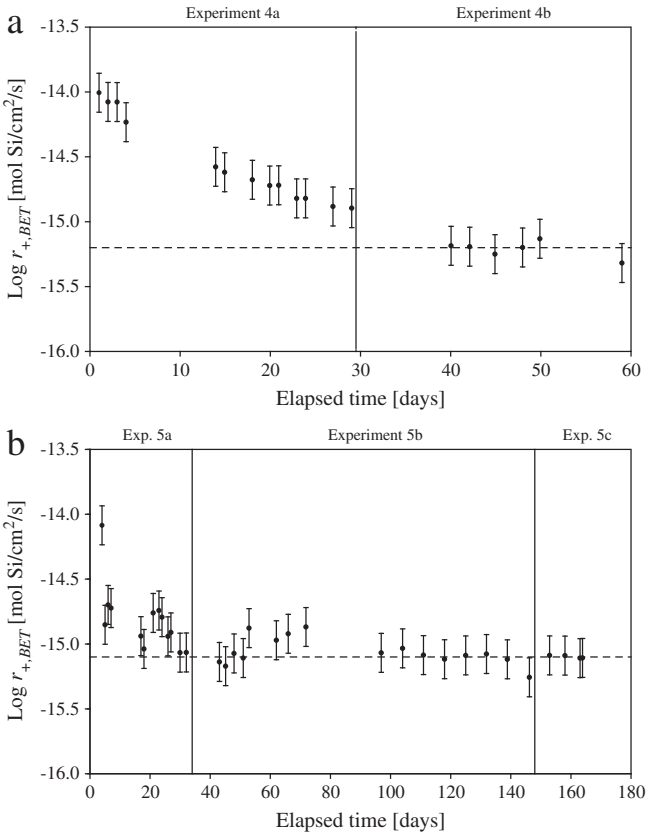

Fig. 3. Measured instantaneous diopside dissolution rates based on Si release during precipitation and control experiments performed at 25 °C and pH 6–8. a) Rates from experiments 4a and b performed in the presence of precipitating calcite. The dashed line corresponds to a final steady-state rate of $10^{-15.2}$. b) Rates from experiments 5a, b and c performed in the absence of precipitating calcite. The dashed line corresponds to a final steady-state rate of $10^{-15.1}$. The error bars on both plots correspond to ±0.15 log units uncertainty on the rates. This uncertainty was based on the scatter among the data points shown in the figure.

3.2. Diopside dissolution in aqueous carbonate inlet fluids at 70 °C (experimental series 1 to 3)

Experimental series 1–3 were originally designed to provoke the precipitation of calcite by the dissolution of diopside in $NaHCO_3$ inlet solutions. Series 1 and 2 dissolved diopside powder at 70 °C in 0.035 mol/kg $NaHCO_3$ and series 3 in 0.010 mol/kg $NaHCO_3$ inlet solutions. Geochemical modeling calculations suggested that the conditions of series 1 and 2 would lead to calcite supersaturation in the reactive fluid and to its precipitation during the experiments. These experiments, however, failed to precipitate carbonate minerals, as evidenced by the saturation state of calcite in the outlet fluid samples, which are all undersaturated with respect to calcite and magnesite (see Table 3), and by analysis of the solids recovered from the experiments by SEM and XRD. As such, all experiments performed in series 1–3 are pure diopside dissolution experiments in the absence of carbonate precipitates.

The temporal evolution of instantaneous diopside dissolution rates based on Si, Ca, and Mg release during experimental series 1–3 is

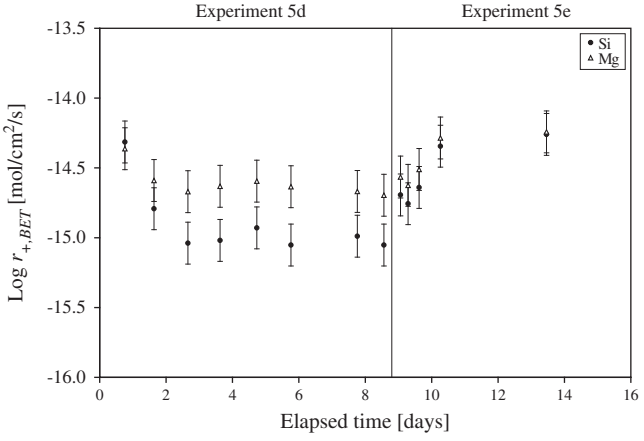

Fig. 4. Measured instantaneous diopside dissolution rates based on Si and Mg release during experiments 5d and e performed at 25 °C and pH 8.5 and pH ~4, respectively. The error bars on both plots correspond to ±0.15 log units uncertainty on the rates. This uncertainty was based on the scatter among the data points shown in the figure.

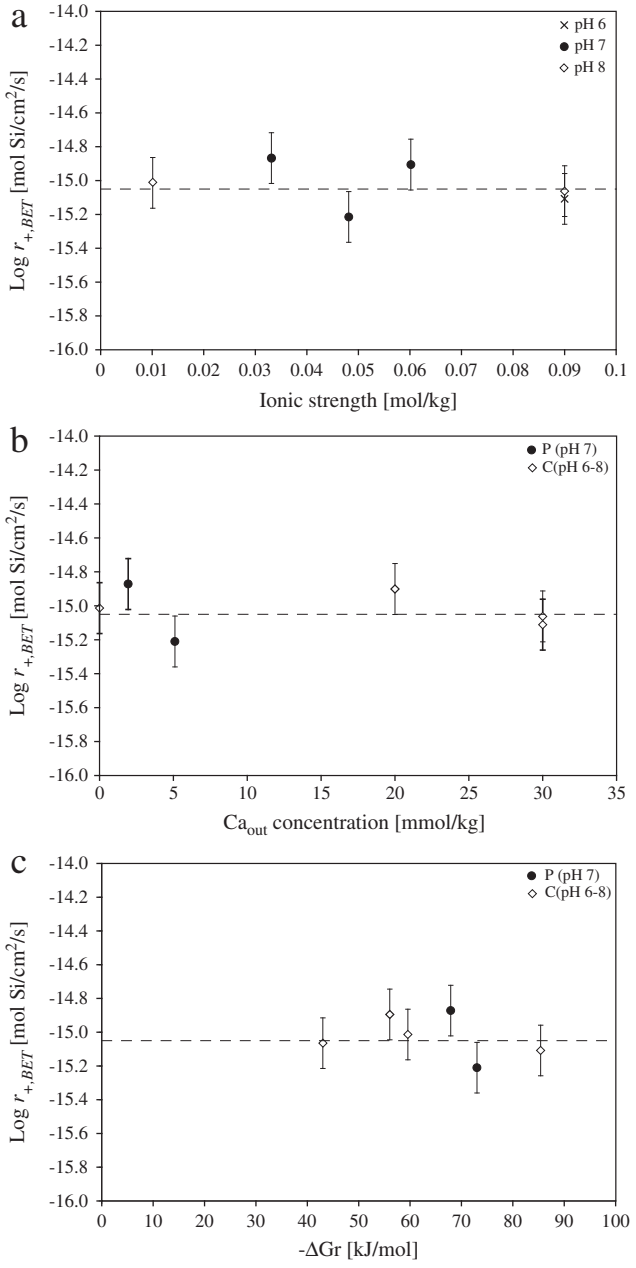

Fig. 5. Measured steady-state diopside dissolution rates based on Si release at pH 6, 7 and 8 as a function of (a) solution ionic strength, (b) reactive fluid Ca concentration of outlet solution, and (c) diopside saturation state. The error bars on these plots correspond to ±0.15 log unit uncertainty. The dashed line in these figures corresponds to a rate of $10^{-15.1}$ mol/cm^2/s. P and C refer to precipitation and control experiments, respectively.

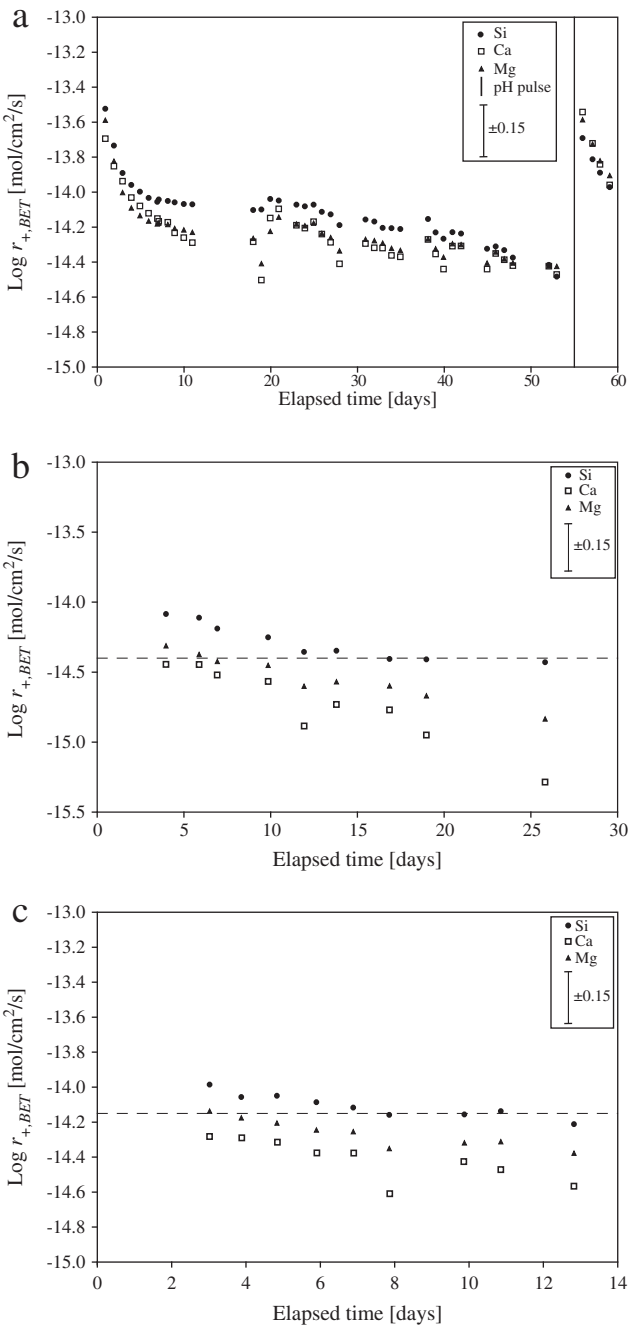

Fig. 6. Measured instantaneous diopside dissolution rates based on Si, Ca, and Mg release during precipitation experiments performed at 70 °C and pH 8.5. a) Rates from experiments 1a and b, where 1b represents a pH-pulse of pH 6.4. b) Rates from experiment 2, and c) rates from experiment 3. The dashed line in plot b) and c) is drawn at a steady-state Si rate at $10^{-14.40}$ mol/cm^2/s and $10^{-14.15}$ mol/cm^2/s, respectively. The uncertainty on the measured rates is ±0.15 log units as illustrated by the error bar in the top-right corner of the plots. This uncertainty was based on the scatter among the data points shown in the figure.

shown in Fig. 6 (see Appendix 1 for a complete list of individual data points). The results shown in this figure indicate that all of these experiments exhibited an initial preferential Si release over Mg and Ca. This preferential Si release attenuates and eventually disappears as the diopside dissolution rates based on Si decrease to match those based on Ca and Mg release after 45 days of dissolution in experiment 1a (see Fig. 6a). This behavior appears to be consistent with the approach to steady state of experiments performed in series 4 and 5. As shown in Figs. 3 and 4, rates based on Si release tend to decrease with time before attaining a steady-state value. Note, similar to previous studies (e.g. Golubev et al., 2005) attainment of steady state in the first experiment in a series took more time than subsequent experiments run on the same powder. A preferential release of Si over Mg and Ca was reported by Knauss et al. (1993) for diopside dissolution at pH 8.9 and 70 °C, though they did not observe a final stoichiometric dissolution phase of their experiments, as they stopped their experiment after 17 days. These results contrast with those obtained at 25 °C which exhibited a preferential release of Mg over Si (see Fig. 4), again consistent with rates reported by Knauss et al. (1993) at pH 7.57 and 25 °C. Oelkers et al. (2009) observed that Si was initially preferentially released from diopside at basic pH, but Mg and Ca were initially preferentially released at acidic pH. A preferential release of Si over Mg was reported in enstatite dissolution experiments performed by Oelkers and Schott (2001) at 70 °C and neutral to basic pH; dissolution eventually became

stoichiometric as Si release rates decreased to equal those of Mg. As further evidence of the lack of carbonate precipitation during these experiments, a HCl pulse of pH 6.4 was added to the inlet fluid at the end of experimental series 1. This pH pulse led to an increase in diopside dissolution rates based on Si, Ca, and Mg release. As rates based of Ca and Mg rates are similar to those based on Si release, and that the rates of carbonate dissolution are far faster than those of diopside at acid pH, it can be concluded that no dissolving carbonate phases were present.

3.3. Fluid saturation states during the experiments

Results of thermodynamic calculations, as listed in Table 3, suggest that some of the outlet fluids at 25 °C were supersaturated with respect to a number of carbonate minerals including calcite, aragonite, dolomite, and dawsonite. The only secondary precipitate observed by SEM, EDS and XRD analysis on post-experimental solids was calcite. In contrast, the outlet fluids of the 70 °C experiments were, in general, undersaturated with respect to these carbonates, and none were observed on the post-experiment solids (see Fig. 1b). Fe-hydroxides (i.e. hematite, goethite), Al-hydroxides (i.e. diaspore, gibbsite), Ti- and Mn oxides, and clay minerals (i.e. nontronite) were also calculated to be supersaturated in experiments performed at 25 and 70 °C. The Fe, Al, Na, Mn, and Ti release rates from the dissolving diopside in this study however, are low so only minor quantities of non-carbonate secondary minerals are likely to have formed, and none were observed with SEM nor EDS on the post-experimental solids (see Fig. 1b–h). Thermodynamic calculations indicate that the outlet fluids were all undersaturated with respect to the dissolving diopside with a chemical affinity; $-\Delta G_r \geq \sim 40$ kJ/mol in all experiments.

4. Discussion

4.1. Comparison with previously published diopside dissolution rates

A comparison of steady-state diopside dissolution rates generated in this study based on Si release and those reported in the literature can be made with the aid of Fig. 7. Rates in this study are consistent with those of Knauss et al. (1993) and Golubev et al. (2005) at 25 °C, and those of Knauss et al. (1993) at 70 °C. All rates tend to decrease mildly with increasing pH, though some of the data sets suggest that this decrease lessens at alkaline conditions at 25 °C. The rates reported by Chen and Brantley (1998) are ~1 order of magnitude lower than corresponding rates reported in other sources. As mentioned above, these authors attributed this difference to differences in the normalizing surface area used in the different studies. Similarly, diopside dissolution rates obtained from experimental series 1–3 at 70 °C are consistent with those of Knauss et al. (1993), as can be seen in Fig 7b.

4.2. Comparison of the effect of carbonate precipitation on diopside versus basaltic glass

Similar coupled dissolution-calcite precipitation experiments were carried out on basaltic glass (Stockmann et al., 2011) and diopside (this study) at 25 °C. In the basaltic glass experiments, calcite mainly formed individual discrete clusters, and only minor $CaCO_3$ crystals were found to precipitate on the glass surface. In contrast, calcite grew extensively on the diopside crystal surfaces in the present study. This difference suggests that diopside is a better nucleation template for calcite than basaltic glass. The difference may stem from the structure of these solids. Glass has a non-ordered silica framework whereas diopside has an ordered monoclinic structure. Diopside dissolution also created a rippled surface (see Fig. 1b), and it can be seen in Fig. 1d and f that these surfaces are favorable calcite precipitation sites. The mode of dissolution may also influence the ability to nucleate and grow secondary precipitates. Both diopside and basaltic glass contain Ca^{2+} and Mg^{2+} that could potentially form carbonates. The lack of carbonate precipitates

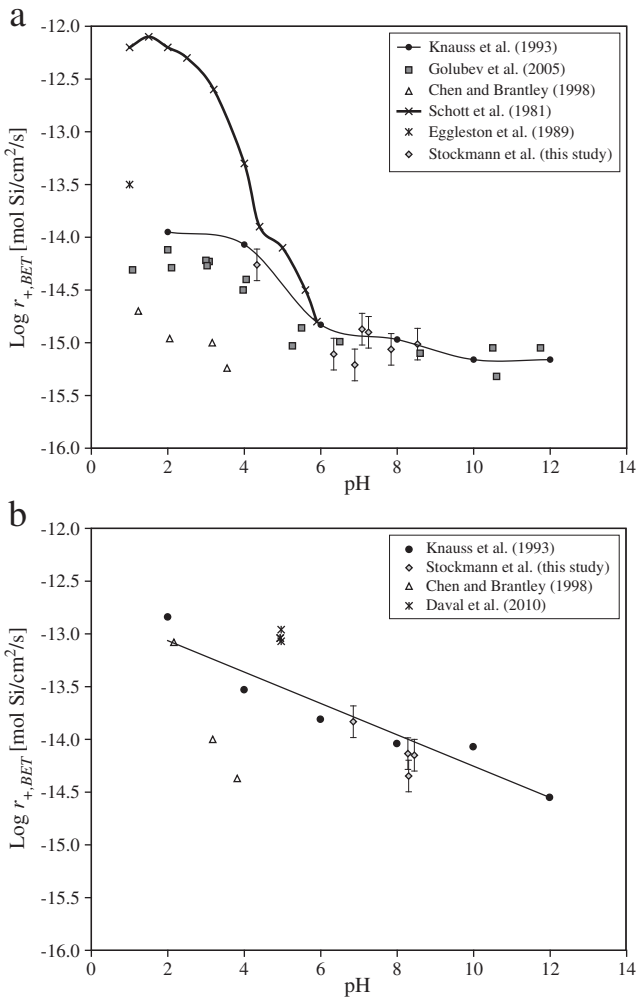

Fig. 7. a) Compilation of diopside dissolution rates based on Si at 20–25 °C reported in the literature and in this study. b) Compilation of diopside dissolution rates near 70 °C reported in the literature and in this study. The data points from Chen and Brantley (1998) and Daval et al. (2010) were measured at 90 °C and based on Si release except for the point at pH 2.16 from Chen and Brantley (1998), which was based on Ca and Mg release. The dashed trend line is based on the plotted data from Knauss et al. (1993).

on the glass suggests that a local source of elements is not itself sufficient to provoke secondary mineral precipitation on the dissolving surface. Another difference between carbonate precipitation in the basaltic glass versus the diopside experiments is that aragonite was also observed to form in the former. As the saturation state of the reactive fluids with respect to aragonite was nearly identical in the basalt and diopside experiments, the observation that aragonite formed in the presence of basaltic glass may be due to the presence of various metals released during glass dissolution. A number of past studies have reported that the formation of aragonite precipitation is favored by the presence of various dissolved trace elements (e.g. Bots et al., 2011).

4.3. Why does calcite precipitation have little effect on diopside dissolution rates?

A major result of this study is that the precipitation of calcite on and near the surfaces of diopside has little effect on its dissolution rates. These results appear to be consistent with the conclusions of Cubillas et al. (2005) who proposed that there will not be an inhibition of dissolution rates of the primary minerals unless there is a close match of the crystallographic properties of the dissolving and precipitating phases leading to epitaxial growth. Other studies suggest that dissolution rates may be inhibited by the formation of amorphous Si layers, as

observed on wollastonite and olivine surfaces (Park and Fan, 2004; Béarat et al., 2006; Andreani et al., 2009; Daval et al., 2009a,b, 2011). The match between the dissolving diopside and the precipitating carbonate in this study appears therefore to be sufficient to promote nucleation on these surfaces yet insufficient to form the impermeable layer required to arrest the dissolution of the primary diopside despite the precipitation of over 5 g of calcite in experimental series 4.

4.4. Implications for carbon storage

This study demonstrates that calcite precipitation does not significantly slow diopside dissolution rates. Stockmann et al. (2011) reported that carbonate precipitation does not affect basaltic glass dissolution rates. These two observations favor carbon storage via the carbonatization of basaltic and ultramafic rocks. This carbonatization process involves the release of Ca, Mg, and Fe from silicate minerals by dissolution. These divalent metals can then react with dissolved CO_2 in the fluid phase to form stable carbonate minerals. It has been argued that silicate mineral dissolution is the slowest and thus rate-limiting step of this coupled process. The observation that calcium carbonate precipitates do not create compact armoring layers on diopside or basaltic glass surfaces suggests that Ca, Mg, and Fe release will not be slowed by carbonate precipitation during mineral sequestration efforts in basalts, as currently being pursued in Iceland and in the Northwest of the United States (McGrail et al., 2006; Alfredsson et al., 2008; Oelkers et al., 2008; Aradóttir et al., 2012b; Schaef and McGrail, 2009; Schaef et al., 2009; Flaathen et al., 2010; Gislason et al., 2010; Schaef et al., 2010; Alfredsson et al., 2011; Aradóttir et al., 2011; Gudbrandsson et al., 2011; Gysi and Stefansson, 2011; Schaef et al., 2011; Aradóttir et al., 2012a; Gysi and Stefansson, 2012a,b,c).

5. Conclusions

The results summarized above suggest that the presence of calcite precipitating on or near the surfaces of diopside does not affect its dissolution rates. Calcite is observed to precipitate both as discrete prisms and as pervasive coatings covering the whole diopside surface. These observations are consistent with those of Cubillas et al. (2005) who concluded that substantial inhibition of mineral dissolution by a precipitating phase is only efficient when there is a close crystal structural match between the dissolving and precipitating phases. The observation that diopside dissolution rates are unaffected by calcite precipitation, favors carbon storage in crystalline basaltic and ultramafic rocks.

Acknowledgments

This study is part of the CarbFix project (www.carbfix.com) in Iceland, and we would like to thank all colleagues and co-workers within this project. We are grateful for technical support provided by Jón Matthíasson at the Innovation Center Iceland, Sophie Gouy at GET-CNRS in Toulouse, France, and David Cornell at Geovetarcentrum, University of Gothenburg in Sweden. We are also indebted to Caroline Piper Hem at the University of Copenhagen for assistance with XRD interpretations. Finally, we would sincerely like to thank Erik Sturkell for graphical assistance and continued support. The Environmental and Energy Fund of Reykjavík Energy, the Research Fund of the University of Iceland, the Nordic Council of Ministers through NORDVULK, and the European Community through the MIN-GRO Research and Training Network (MRTN-CT-2006-035488), the CarbFix project (Collaborative project-FP7-ENERGY-2011-1-283148) and the ERASMUS student mobility program are gratefully acknowledged for their financial support. We are grateful for the useful comments provided by the editor Professor Uwe Brand and two anonymous reviewers, which improved the manuscript.

Appendix 1. Diopside dissolution rates (mol/cm^2/s) based on Si, Ca and Mg release at 70 °C

Exp. no.	Elapsed time, days	pH, 70 °C	log $r_{+,Si,BET}$	log $r_{+,Ca,BET}$	log $r_{+,Mg,T}$	ΔG_r^a	log $(a^2_{H^+}/a_{Ca^{2+}})$ [a]	log $(a^2_{H^+}/a_{Mg^{2+}})$ [a]
			Si	Ca	Mg	Diopside		
			mol/cm^2/s	mol/cm^2/s	mol/cm^2/s	kJ/mol		
Experiment 1a–b at 70 °C, diopside dissolution in a 0.035 mol/kg $NaHCO_3$ inlet solution								
D-1	0.9	8.34	−13.52	−13.69	−13.59	−21.92	−11.29	−11.59
D-2	1.9	8.36	−13.73	−13.85	−13.82	−26.88	−11.15	−11.40
D-3	2.9	8.38	−13.89	−13.94	−14.00	−30.32	−11.09	−11.25
D-4	3.9	8.39	−13.96	−14.03	−14.09	−32.25	−11.02	−11.18
D-5	4.9	8.44	−14.00	−14.08	−14.13	−32.33	−11.05	−11.23
D-6	5.9	8.43	−14.03	−14.12	−14.17	−33.40	−10.99	−11.19
D-7	6.9	8.47	−14.06	−14.15	−14.18	−33.36	−11.01	−11.23
D-8	7.1	8.47	−14.04	−14.17	−14.18	−33.31	−11.00	−11.23
D-9	8.1	8.50	−14.05	−14.17	−14.19	−32.91	−11.04	−11.27
D-10	8.9	8.49	−14.06	−14.23	−14.21	−33.77	−10.96	−11.23
D-11	10.0	8.52	−14.07	−14.26	−14.22	−33.49	−10.98	−11.29
D-12	11.0	8.56	−14.07	−14.29	−14.23	−33.15	−11.01	−11.33
D-13	18.0	8.56	−14.10	−14.28	−14.26	−33.71	−11.02	−11.30
D-14	18.9	8.55	−14.10	−14.50	−14.41	−36.49	−10.76	−11.13
D-15	19.9	8.36	−14.04	−14.15	−14.22	−35.66	−10.85	−10.97
D-16	20.9	8.36	−14.05	−14.10	−14.14	−34.85	−10.91	−11.06
D-17	23.0	8.53	−14.07	−14.19	−14.18	−32.70	−11.07	−11.33
D-18	23.9	8.43	−14.08	−14.21	−14.19	−34.93	−10.91	−11.13
D-19	24.9	8.42	−14.07	−14.17	−14.18	−34.52	−10.93	−11.15
D-20	25.9	8.46	−14.11	−14.24	−14.24	−35.25	−10.92	−11.15
D-21	26.9	8.44	−14.13	−14.29	−14.26	−36.20	−10.84	−11.10
D-22	27.9	8.49	−14.19	−14.41	−14.34	−37.36	−10.80	−11.11
D-23	30.9	8.39	−14.16	−14.29	−14.27	−37.64	−10.76	−11.01
D-24	31.9	8.42	−14.17	−14.32	−14.28	−37.52	−10.76	−11.05
D-25	32.9	8.56	−14.20	−14.32	−14.29	−35.57	−10.98	−11.27
D-26	33.9	8.43	−14.21	−14.36	−14.32	−38.29	−10.76	−11.01
D-27	34.9	8.47	−14.21	−14.37	−14.33	−37.84	−10.79	−11.08
D-28	38.1	8.44	−14.15	−14.27	−14.27	−36.52	−10.86	−11.09
D-29	39.0	8.49	−14.23	−14.35	−14.32	−37.69	−10.84	−11.10
D-30	39.9	8.51	−14.27	−14.44	−14.37	−38.58	−10.78	−11.11
D-31	40.9	8.41	−14.23	−14.31	−14.29	−38.67	−10.77	−11.00
D-32	41.9	8.41	−14.24	−14.31	−14.30	−38.64	−10.77	−11.01
D-33	44.9	8.50	−14.32	−14.44	−14.41	−39.80	−10.77	−11.06
D-34	45.9	8.53	−14.31	−14.35	−14.34	−37.90	−10.91	−11.19
D-35	46.9	8.37	−14.33	−14.39	−14.38	−41.73	−10.62	−10.87
D-36	47.9	8.47	−14.37	−14.42	−14.41	−40.82	−10.74	−11.00
D-37	52.1	8.37	−14.42	−14.42	−14.42	−43.29	−10.59	−10.82
D-38	53.0	8.37	−14.48	−14.47	−14.42	−44.53	−10.53	−10.82
D-39	55.9	6.70	−13.69	−13.54	−13.59	−61.61	−8.52	−8.49
D-40	57.1	6.73	−13.81	−13.72	−13.73	−64.47	−8.40	−8.42
D-41	58.0	6.83	−13.89	−13.84	−13.82	−64.35	−8.48	−8.52
D-42	59.1	7.19	−13.97	−13.96	−13.91	−57.58	−9.06	−9.14
Experiment 2 at 70 °C, diopside dissolution in a 0.035 mol/kg $NaHCO_3$ inlet solution								
D-100	4.0	8.39	−14.08	−14.44	−14.31	−38.09	−10.59	−10.93
D-101	5.9	8.25	−14.11	−14.45	−14.37	−41.54	−10.39	−10.66
D-102	6.9	8.29	−14.19	−14.52	−14.42	−42.53	−10.38	−10.68
D-103	9.9	8.22	−14.25	−14.57	−14.45	−45.48	−10.21	−10.51
D-104	11.9	8.30	−14.36	−14.89	−14.60	−48.67	−9.99	−10.48
D-105	13.8	8.24	−14.35	−14.73	−14.57	−48.09	−10.09	−10.44
D-106	16.9	8.24	−14.41	−14.77	−14.60	−49.65	−10.04	−10.37
D-107	19.0	8.35	−14.41	−14.95	−14.67	−48.97	−10.05	−10.48
D-108	25.8	8.51	−14.43	−15.29	−14.83	−49.41	−9.90	−10.67
Experiment 3 at 70 °C, diopside dissolution in a 0.010 mol/kg $NaHCO_3$ inlet solution.								
D-200	3.0	8.29	−13.99	−14.28	−14.14	−49.02	−10.31	−10.56
D-201	3.9	8.35	−14.06	−14.29	−14.18	−49.06	−10.39	−10.63
D-202	4.8	8.23	−14.05	−14.31	−14.21	−51.96	−10.17	−10.38
D-203	5.9	8.28	−14.09	−14.38	−14.24	−51.98	−10.19	−10.44
D-204	6.9	8.30	−14.12	−14.38	−14.25	−52.07	−10.23	−10.47
D-205	7.9	8.33	−14.16	−14.61	−14.35	−54.06	−10.05	−10.42

Appendix Table (*continued*)

Exp. no.	Elapsed time, days	pH, 70 °C	log $r_{+,\text{Si, BET}}$	log $r_{+,\text{Ca, BET}}$	log $r_{+,\text{Mg,T}}$	ΔG_r^a	log $(a^2_{H^+}/a_{Ca^{2+}})$ [a]	log $(a^2_{H^+}/a_{Mg^{2+}})$ [a]
			Si	Ca	Mg	Diopside		
			mol/cm^2/s	mol/cm^2/s	mol/cm^2/s	kJ/mol		
D-206	9.9	8.21	−14.16	−14.43	−14.32	−55.50	−10.02	−10.22
D-207	10.9	8.26	−14.14	−14.47	−14.31	−54.16	−10.07	−10.34
D-208	12.8	8.34	−14.21	−14.56	−14.38	−54.34	−10.12	−10.41

[a]Computed using PHREEQC version 2.17.

References

Alfredsson, H.A., Hadrarson, B.S., Franzson, H., Gislason, S.R., 2008. CO_2 sequestration in basaltic rock at the Hellisheidi site in SW Iceland: stratigraphy and chemical composition of the rocks at the injection site. Mining Magazine 72, 1–5.

Alfredsson, H.A., Wolff-Boenisch, D., Stefansson, A., 2011. CO_2 sequestration in basaltic rocks in Iceland: development of a piston-type downhole sampler for CO_2 rich fluids and tracers. Energy Procedia 4, 3510–3517.

Andreani, M., Liquot, L., Gouze, P., Godard, M., Hoise, E., Gibert, B., 2009. Experimental study of carbon sequestration reactions controlled by the percolation of CO_2-rich brine through peridotites. Environmental Science & Technology 43, 1226–1231.

Aradóttir, E.S.P., Sigurdardóttir, H., Sigfússon, B., Gunnlaugsson, E., 2011. CarbFix — a CCS pilot project imitating and accelerating natural CO_2 sequestration. Greenhouse Gases: Science and Technology 1, 105–118.

Aradóttir, E.S.P., Sonnenthal, E.L., Jónsson, H.I., 2012a. Development and evaluation of a thermodynamic dataset for phases of interest in CO_2 sequestration in basaltic rocks. Chemical Geology 304–305, 26–38.

Aradóttir, E.S.P., Sonnenthal, E.L., Björnsson, G., Jónsson, H., 2012b. Multidimensional reactive transport modeling of CO_2 mineral sequestration in basalts at the Hellisheidi geothermal field, Iceland. International Journal of Greenhouse Gas Control 9, 24–40.

Béarat, H., McKelvey, M.J., Chizmeshya, A.V., Gormley, D., Nunez, R., Carpenter, R.W., Squires, K., Wolf, G.H., 2006. Carbon sequestration via aqueous olivine mineral carbonation: role of passivating layer formation. Environmental Science & Technology 40, 4802–4808.

Bots, P., Benning, L.G., Rickaby, R.E.M., Shaw, S., 2011. The role of SO_4 in the switch from calcite to aragonite seas. Geology 39, 331–334.

Chaïrat, C., Schott, J., Oelkers, E.H., Lartigue, J.-E., Harouiya, N., 2007. Kinetics and mechanism of natural fluorapatite dissolution at 25 °C and pH from 3 to 12. Geochimica et Cosmochimica Acta 71, 5901–5912.

Chen, Y., Brantley, S.L., 1998. Diopside and anthophyllite dissolution at 25° and 90 °C and acid pH. Chemical Geology 147, 233–248.

Cubillas, P., Köhler, S., Prieto, M., Causserand, C., Oelkers, E.H., 2005. How do mineral coatings affect dissolution rates? An experimental study of coupled $CaCO_3$ dissolution–$CdCO_3$ precipitation. Geochimica et Cosmochimica Acta 69, 5459–5476.

Daval, D., Martinez, I., Corvisier, J., Findling, N., Goffe, B., Guyot, F., 2009a. Carbonation of Ca-bearing silicates, the case of wollastonite: experimental investigations and kinetic modeling. Chemical Geology 265, 63–78.

Daval, D., Martinez, I., Guigner, J.-M., Hellmann, R., Corvisier, J., Findling, N., Dominici, C., Goffe, B., Guyot, F., 2009b. Mechanism of wollastonite carbonation deduced from micro- to nanometer length scale observations. American Mineralogist 94, 1707–1726.

Daval, D., Hellmann, R., Corvisier, J., Tisserand, D., Martinez, I., Guyot, F., 2010. Dissolution kinetics of diopside as a function of solution saturation state: macroscopic measurements and implications for modeling of geological storage of CO_2. Geochimica et Cosmochimica Acta 74, 2615–2633.

Daval, D., Sissmann, O., Menguy, N., Saldi, G.D., Guyot, F., Martinez, I., Corvisier, J., Garcia, B., Machouk, I., Knauss, K.G., Hellmann, R., 2011. Influence of amorphous silica layer formation on the dissolution rate of olivine at 90 °C and elevated pCO_2. Chemical Geology 284, 193–209.

Dixit, S., Caroll, S.A., 2007. Effect of solution saturation state and temperature on diopside dissolution. Geochemical Transactions. http://dx.doi.org/10.1186/1467-4866-8-3.

Eggleston, C.M., Hochella Jr., M.F., George, P.A., 1989. Sample preparation and aging effects on the dissolution rate and surface composition of diopside. Geochimica et Cosmochimica Acta 53, 797–804.

Flaathen, T.K., Gislason, S.R., Oelkers, E.H., 2010. The effect of aqueous sulphate on basaltic glass dissolution rates. Chemical Geology 277, 345–354.

Gautelier, M., Oelkers, E.H., Schott, J., 2007. An experimental study of dolomite dissolution rates at 80 °C as a function of chemical affinity and solution composition. Chemical Geology 242, 509–517.

Giammar, D.E., Bruant Jr., R.G., Peters, C.A., 2005. Forsterite dissolution and magnesite precipitation at conditions relevant for deep saline aquifer storage and sequestration of carbon dioxide. Chemical Geology 217, 257–276.

Gislason, S.R., Wolff-Boenisch, D., Stefansson, A., Oelkers, E.H., Gunnlaugsson, E., Sigurdardóttir, H., Sigfússon, G., Brocker, W.S., Matter, J., Stute, M., Axelsson, G., Fridriksson, T., 2010. Mineral sequestration of carbon dioxide in basalt: a pre-injection overview of the CarbFix project. International Journal of Greenhouse Gas Control 4, 537–545.

Goldberg, D.S., Takahashi, T., Slagle, A.L., 2008. Carbon dioxide sequestration in deep-sea basalt. Proceedings of the National Academy of Sciences 105, 9920–9925.

Golubev, S.V., Pokrovsky, O.S., 2006. Experimental study of the effect of organic ligands on diopside dissolution kinetics. Chemical Geology 235, 377–389.

Golubev, S.V., Pokrovsky, O.S., Schott, J., 2005. Experimental determination of the effect of dissolved CO_2 on the dissolution kinetics of Mg and Ca silicates at 25 °C. Chemical Geology 217, 227–238.

Gudbrandsson, S., Wolff-Boenisch, D., Gislason, S.R., Oelkers, E.H., 2011. An experimental study of crystalline basalt dissolution from $2 \leq pH \leq 11$ and temperatures from 5 to 75 °C. Geochimica et Cosmochimica Acta 75, 5496–5509.

Gysi, A.P., Stefansson, A., 2011. CO_2–water–basalt interaction. Numerical simulation of low temperature CO_2 sequestration into basalts. Geochimica et Cosmochimica Acta 75, 4728–4751.

Gysi, A.P., Stefansson, A., 2012a. CO_2-water-basalt interaction. Low temperature experiments and implications for CO_2 sequestration into basalts. Geochimica et Cosmochimica Acta 81, 129–152.

Gysi, A.P., Stefansson, A., 2012b. Mineralogical aspects of CO_2 sequestration during hydrothermal basalt alteration — an experimental study at 75 to 250 °C and elevated pCO_2. Chemical Geology 306–307, 146–159.

Gysi, A.P., Stefansson, A., 2012c. Experiments and geochemical modeling of CO_2 sequestration during hydrothermal basalt alteration. Chemical Geology 306–307, 10–28.

Helgeson, H.C., Murphy, W.M., Aagaard, P., 1984. Thermodynamic and kinetic constraints on reaction rates among minerals and aqueous solutions. II. Rate constants, effective surface area, and the hydrolysis of feldspars. Geochimica et Cosmochimica Acta 48, 2405–2432.

Hodson, M.E., 2003. The influence of Fe-rich coatings on the dissolution of anorthite at pH 2.6. Geochimica et Cosmochimica Acta 67, 3355–3363.

Kelemen, P.B., Matter, J., 2008. In situ carbonation of peridotite for CO_2 storage. PNAS 105, 17295–17300.

Klein, C., 2002. Manual of Mineral Science, 22nd edition. John Wiley & Sons, Inc., New York (642 pp.).

Knauss, K.G., Nguyen, S.N., Weed, H.C., 1993. Diopside dissolution kinetics as a function of pH, CO_2, temperature, and time. Geochimica et Cosmochimica Acta 57, 285–294.

Lasaga, A.C., 1984. Chemical kinetics of water–rock interactions. Journal of Geophysical Research 89 (B6), 4009–4025.

Marini, L., 2007. Geological sequestration of carbon dioxide. Thermodynamics, Kinetics and Reaction Path modeling. Elsevier, Amsterdam (470 pp.).

Matter, J.M., Takahashi, T., Goldberg, D., 2007. Experimental evaluation of in-situ CO_2–water–rock reactions during CO_2 injection in basaltic rocks: Implications for geological CO_2 sequestration. Geochemistry, Geophysics, Geosystems 8, Q02001. http://dx.doi.org/10.1029/2006GC001427.

Matter, J.M., Broecker, W.S., Gislason, S.R., Gunnlaugsson, E., Oelkers, E.H., Stute, M., Sigurdardóttir, H., Stefansson, A., Alfredsson, H.A., Aradóttir, E.S., Axelsson, G., Sigfusson, B., Wolff-Boenisch, D., 2011. The CarbFix pilot project — storing carbon dioxide in basalt. Energy Procedia 4, 5579–5585.

McGrail, B.P., Schaef, H.T., Ho, A.M., Chien, Yi-Ju, Dooley, J.J., Davidson, C.L., 2006. Potential for carbon dioxide sequestration in flood basalts. Journal of Geophysical Research 111, B12201. http://dx.doi.org/10.1029/2005JB004169.

Oelkers, E.H., 2001. General kinetic description of multioxide silicate mineral and glass dissolution. Geochimica et Cosmochimica Acta 65, 3703–3719.

Oelkers, E.H., Cole, D.R., 2008. Carbon dioxide sequestration: a solution to a global problem. Elements 4, 305–310.

Oelkers, E.H., Schott, J., 2001. An experimental study of enstatite dissolution rates as a function of pH, temperature, and aqueous Mg and Si concentration, and the mechanism of pyroxene/pyroxenoid dissolution. Geochimica et Cosmochimica Acta 65, 1219–1231.

Oelkers, E.H., Schott, J., 2005. Geochemical aspects of CO_2 sequestration. Chemical Geology 217, 183–186.

Oelkers, E.H., Gislason, S.R., Matter, J., 2008. Mineral carbonation of CO_2. Elements 4, 333–337.

Oelkers, E.H., Golubev, S.V., Chairat, C., Pokrovsky, O.S., Schott, J., 2009. The surface chemistry of multi-oxide silicates. Geochimica et Cosmochimica Acta 73, 4617–4634.

Pačes, T., 1983. Rate constants of dissolution derived from the measurements of mass balance in hydrological catchments. Geochimica et Cosmochimica Acta 47, 1855–1863.

Park, A.-H.A., Fan, L.-S., 2004. CO_2 mineral sequestration: physically activated dissolution of serpentine and pH swing process. Chemical Engineering Science 59, 5241–5247.

Parkhurst, D.L., Appelo, C.A.J., 1999. User's guide to PHREEQC (Version 2) — a computer program for speciation, batch-reaction, one-dimensional transport, and inverse geochemical calculations. USGS-Report 99–4259.

Pokrovsky, O.S., Schott, J., Castillo, A., 2005. Kinetics of brucite dissolution at 25 °C in the presence of organic and inorganic ligands and divalent metals. Geochimica et Cosmochimica Acta 69, 905–918.

Putnis, A., 2009. Mineral replacement reactions. Reviews in Mineralogy and Geochemistry 70, 87–124.

Rudge, J.F., Kelemen, P.B., Spiegelman, M., 2011. A simple model of reaction-induced cracking applied to serpentinization and carbonation of peridotite. Earth and Planetary Science Letters 291, 215–227.

Schaef, H.T., McGrail, B.P., 2009. Dissolution of Columbia River Basalt under mildly acidic conditions as a function of temperature: Experimental results relevant to the geological sequestration of carbon dioxide. Applied Geochemistry 24, 980–987.

Schaef, H.T., McGrail, B.P., Owen, A.T., 2009. Basalt–CO_2–H_2O interactions and variability in carbonate mineralization rates. Energy Procedia 1, 4899–4906.

Schaef, H.T., McGrail, B.P., Owen, A.T., 2010. Carbonate mineralization of volcanic province basalts. International Journal of Greenhouse Gas Control 4, 249–261.

Schaef, H.T., McGrail, B.P., Owen, A.T., 2011. Basalt reactivity variability with reservoir depth in supercritical CO_2 and aqueous phases. Energy Procedia 4, 4977–4984.

Schott, J., Oelkers, E.H., 1995. Dissolution and crystallization rates of silicate minerals as a function of chemical affinity. Pure and Applied Chemistry 67, 903–910.
Schott, J., Berner, R.A., Sjöberg, E.L., 1981. Mechanism of pyroxene and amphibole weathering—I. Experimental studies of iron-free minerals. Geochimica et Cosmochimica Acta 45, 2123–2135.
Schott, J., Pokrovsky, O.S., Oelkers, E.H., 2009. The link between mineral dissolution/precipitation kinetics and solution chemistry. Reviews in Mineralogy and Geochemistry 70, 207–258.
Siegel, D.I., Pfannkuch, H.O., 1984. Silicate dissolution influence on Filson Creek chemistry, northeastern Minnesota. Geological Society of America Bulletin 95, 1446–1453.
Stockmann, G.J., Wolff-Boenisch, D., Gislason, S.R., Oelkers, E.H., 2011. Do carbonate precipitates affect dissolution kinetics? 1: basaltic glass. Chemical Geology 284, 306–316.
Velbel, M.A., 1993. Formation of protectiye surface layers during silicate-mineral weathering under well-leached oxidizing conditions. American Mineralogist 78, 405–414.
Wakahama, H., Mito, S., Ohsumi, T., Ueda, A., Yajima, T., Satoh, H., Sugiyama, K., Ozawa, A., Ajima, S., Todaka, N., Sato, T., Kato, M., Kaji, Y., Tokumarui, T., Kaieda, H., Kubota, K., 2009. A concept of CO_2 georeactor sequestration at the Ogachi HDR site, NE Japan. Energy Procedia 3683–3689.
Wolff-Boenisch, D., Gislason, S.R., Oelkers, E.H., Putnis, C.V., 2004a. The dissolution rates of natural glasses as a function of their composition at pH 4 and 10.6, and temperatures from 25 to 74 °C. Geochimica et Cosmochimica Acta 68, 4843–4858.
Wolff-Boenisch, D., Gislason, S.R., Oelkers, E.H., 2004b. The effect of fluoride on the dissolution rates of natural glasses at pH 4 and 25 °C. Geochimica et Cosmochimica Acta 68, 4571–4582.
Wolff-Boenisch, D., Gislason, S.R., Oelkers, E.H., 2006. The effect of crystallinity on dissolution rates and CO_2 consumption capacity of silicates. Geochimica et Cosmochimica Acta 70, 858–870.
Wolff-Boenisch, D., Wenau, S., Gislason, S.R., Oelkers, E.H., 2011. Dissolution of basalts and peridotite in seawater, in the presence of ligands, and CO_2: implications for mineral sequestration of carbon dioxide. Geochimica et Cosmochimica Acta 75, 5510–5525.